Draft version December 14, 2019
Typeset using LaTeX **twocolumn** style in AASTeX62

Non-equilibrium temperature evolution of ionization fronts during the Epoch of Reionization

Chenxiao Zeng[1,2] and Christopher M. Hirata[1,2,3]

[1] *Center for Cosmology and Astroparticle Physics (CCAPP)*
The Ohio State University, Columbus, OH 43210, USA
[2] *Department of Physics, The Ohio State University, Columbus, OH 43210, USA*
[3] *Department of Astronomy, The Ohio State University, Columbus, OH 43210, USA*

(Received XXX; Revised YYY; Accepted ZZZ)

ABSTRACT

The epoch of reionization (EoR) marks the end of the Cosmic Dawn and the beginning of large-scale structure formation in the universe. The impulsive ionization fronts (I-fronts) heat and ionize the gas within the reionization bubbles in the intergalactic medium (IGM). The temperature during this process is a key yet uncertain ingredient in current models. Typically, reionization simulations assume all baryon particles reach equilibrium states immediately as supersonic I-front propagating through the IGM. Here we present a new model of the temperature evolution for the ionization front by studying non-equilibrium effects. In particular, we include the energy transfer between major baryon species (e^-, H I, H II, He I, and He II) and investigate their impacts on the post-ionization front temperature $T_{\rm re}$. For a better step-size control when solving the stiff equations, we implement an implicit method and construct an energy transfer rate matrix. We find that the assumption of equilibration is valid for a low-speed ionization front ($\lessapprox 10^9$ cm/s), but deviations from equilibrium occur for faster fronts. The post-front temperature $T_{\rm re}$ is lower by up to 1% (at 3×10^9 cm/s) or 7% (at 10^{10} cm/s) relative to the equilibrium case.

Keywords: cosmology: theory — intergalactic medium — reionization, first stars

1. INTRODUCTION

The Epoch of Reionization (EoR) is the process when ultraviolet (UV) photons from the first stars ionized almost all of the neutral hydrogen in the intergalactic medium (IGM). This transition is thought to occur around $z\sim6-12$ (Becker et al. 2001; Fan et al. 2006; McGreer et al. 2015; Planck Collaboration et al. 2018).

Temperature evolution of the IGM is one of the key ingredients in any reionization model, constraining the source energy and injection processes into the IGM. In the standard theory, as ionization fronts (I-fronts) propagate outward from ionization sources, a sharp boundary between ionized particles and neutrals forms (McQuinn 2016). As I-fronts passing through, the IGM gas are rapidly heated to the order of 10^4K (Miralda-Escudé & Rees 1994; Hui, & Gnedin 1997; Hirata 2018; D'Aloisio et al. 2019) which is so-called post-ionization-front temperature $T_{\rm re}$. The heated IGM then undergoes a cooling process by the joint effects of adiabatic expansion of the universe and inverse Compton scattering with Cosmic Microwave Background (CMB) photons.

There is a great uncertainty on the post-ionization temperature $T_{\rm re}$, due to the difficulty of simulating and measuring the thermal evolution history. Experiments estimate the volume-weighted mean temperature of the IGM during EoR by measuring thermal broadening of Lyman-alpha (Lyα) forest absorption features (Schaye et al. 2000; Lidz et al. 2010; Becker et al. 2011; Garzilli et al. 2012; Rudie et al. 2012; Boera et al. 2014; Bolton et al. 2014). An example of simulating $T_{\rm re}$ is shown in D'Aloisio et al. (2019), where they used high-resolution radiative transfer (RT) simulations. In their work, $T_{\rm re}$ mildly depends on incident spectrum and primarily sensitive to the I-front speeds. One approximation they made is that all baryon species reach equilibration states instantaneously as I-front passing through. This is assuming the timescale of thermalizing baryon species other than photoelectrons is small compared with the time that gas stays in the I-front. However, it is possible that non-equilibrium effects can influence the thermal evolution in the I-front. This is because if the front speed is large enough, the local gas density is low and

the energy-transfer interaction rates become comparable with the timescale that gas stay in the I-front.

In this paper, we build a non-equilibrium model of $T_{\rm re}$ by coupling an implicit stiff solver to the 1-dimensional grid-based I-front model of Hirata (2018). We solve a set of stiff equations describing the energy transfer between species after photoelectrons are thermalized at each time step. Adding interactions, both $T_{\rm re}$ and equilibrium states in the I-front are affected. The source code is placed in a public GitHub repository[1].

This paper is structured as follows. In Section 2, we briefly review the one-dimensional grid model. In Section 3, we present our stiff solver algorithm in detail and explain the energy transfer cross sections between species in four categories. In Section 4, we build the dependence of $T_{\rm re}$ on the incident blackbody spectrum $T_{\rm bb}$ and I-front speed v_i when non-equilibrium effects are present. We conclude in Section 5.

2. METHOD: GRID MODEL

Here we review the grid model for temperature evolution during the epoch of reionization. We only summarize the main results of the model, and detailed derivations are explained in the appendix of Hirata (2018). Following the physical reasoning of Miralda-Escudé & Rees (1994), this model describes density-dependent reionization temperature $T_{\rm re}$.

The model is a time-dependent ionization front in one dimension with the depth parameter $N_{\rm H}$ (units: cm^{-2}) the total hydrogen column. The ionization front is built on a grid of $N_{\rm grid}$ cells of width $\Delta N_{\rm H}$, and each cell $j \in \{0, ..., N_{\rm grid}\}$ contains a hydrogen neutral fraction $y_{{\rm HI},j}$, a helium neutral fraction $y_{{\rm HeI},j}$, and an energy per hydrogen nucleus E_j. We consider only the first ionization front, i.e., H I/He I→H II/He II; the He II→He III ionization occurs later [+ref] and is not treated in this paper.

A flux of photons F (units: photons cm^{-2} s^{-1} **[Check updated unit]**) incidents on the left side of the grid. The ionization front has velocity $v_i = F(1 - v_i/c)/[n_{\rm H}(1 + f_{\rm He})]$, where $n_{\rm H}$ is the three-dimensional hydrogen number density and $f_{\rm He}$ is the helium-to-hydrogen ratio. The relativistic correction term v_i/c accounts for the finite time that incident photons travel to the I-front. To visualize the temperature in terms of the total hydrogen column $N_{\rm H}$, we introduce a rescaled time $t' \equiv Ft$ (units: photons cm^{-2}).

Breaking the incident flux into a set of wavelength bins λ, the photoionization rates for hydrogen and helium are

$$\frac{dy_{{\rm HI},j}}{dt'} = \sum_\lambda A_{j\lambda} \frac{\tau_{j\lambda}^{\rm HI}}{\tau_{j\lambda}^{\rm HI} + \tau_{j\lambda}^{\rm HeI}} \tag{1}$$

$$\frac{dy_{{\rm HeI},j}}{dt'} = \sum_\lambda \frac{1}{f_{\rm He}} A_{j\lambda} \frac{\tau_{j\lambda}^{\rm HeI}}{\tau_{j\lambda}^{\rm HI} + \tau_{j\lambda}^{\rm HeI}}, \tag{2}$$

where $\tau_{j\lambda}^{\rm HI} = \Delta N_{\rm H} y_{{\rm HI},j} \sigma_\alpha^{\rm HI}/(1 - v_i/c)$ and $\tau_{j\lambda}^{\rm HeI} = f_{\rm He} \Delta N_{\rm H} y_{{\rm HeI},j} \sigma_\alpha^{\rm HeI}/(1 - v_i/c)$ are optical depths to photons in frequency bin λ. The same relativistic correction term as in F indicates that the grid width should be broaden for I-front moving close to the speed of light. Here $\mathcal{A}_{j\lambda}$ is the number of absorbed photons per hydrogen nucleus per rescaled time. **[Give formula for $\mathcal{A}_{j\lambda}$]**

The photoionization and collisional cooling lead to a net heating rate

$$\frac{dE_j}{dt'} = \sum_\lambda \mathcal{A}_{j\lambda} \frac{\tau_{j\lambda}^{\rm HI} (h\nu - I_{\rm HI}) + \tau_{j\lambda}^{\rm HeI} (h\nu - I_{\rm HeI})}{\tau_{j\lambda}^{\rm HI} + \tau_{j\lambda}^{\rm HeI}} - \frac{y_{{\rm HI},j} x_{e,j} (1 - v_i/c)}{v_i (1 + f_{\rm He})} \sum_{n=2}^{3} q_{1\to n} h\nu_1 \left(1 - n^{-2}\right), \tag{3}$$

where E_j is the thermal energy per hydrogen nucleus in grid cell j, $x_{e,j}$ is the energy-temperature conversion factor defined in Table 1, and $q_{1\to n}$ represents the collisional excitation rate coefficient (units: cm^{3}s^{-1}) for exciting a hydrogen atom to the nth level. $I_{\rm HI}$ and $I_{\rm HeI}$ are the ionization energies. **[should we call the frequency $\nu_\lambda = c/\lambda$ instead of ν, since it depends on the bin?]**

The major baryonic components of the IGM are e^-, H I , H II , He I , and He II. In what follows, we use the subscripts $\alpha, \beta, ...$ to denote these components, and Latin indices $j, ...$ to denote grid cells. **[Do we want to write j everywhere or is this distracting?]** We write the energy in component α per hydrogen nucleus as E_α, and its temperature as

$$T_\alpha = \frac{2E_\alpha}{3k_{\rm B} f_\alpha}, \tag{4}$$

where $f_\alpha = n_\alpha/n_{\rm H}$ is the abundance of that species relative to total hydrogen nuclei. These factors are listed in Table 1. The assumption of equilibrium states that all these temperatures are equal, in which case

$$T = \frac{2E}{3k_{\rm B} \sum_\alpha f_\alpha}. \tag{5}$$

[1] https://github.com/frankelzeng/reionization

Table 1. Energy-temperature conversion factors.

e^-: f_1	H I: f_2	H II: f_3	He I: f_4	He II: f_5
x_e	$y_{\rm HI}$	$1-y_{\rm HI}$	$f_{\rm He}y_{\rm He}$	$f_{\rm He}(1-y_{\rm He})$

Note — For electrons, $x_e = 1 - y_{\rm HI} + f_{\rm He}(1-y_{\rm He})$.

3. METHOD: STIFF SOLVER FOR INTERACTIONS

We extend the equilibrium (electron-only) grid model by investigating the temperature evolution of five species (e^-, H I , H II , He I , and He II) separately. This requires us to study the mutual interactions and energy exchange within different species in the IGM. We only include two-body interactions, which can be represented by $\binom{5}{2} = 10$ interaction rates. The system of equations is considered stiff because some of the energy transfer rates are large compared with the time scale of the overall reionization process, indicating an unacceptably small step size when doing integration. In this work, we construct an implicit stiff solver to reflect the temperatures evolution. We make an approximation that the species equilibrate among themselves immediately because this process is much faster than that within different components (e.g., electron-ion or ion-ion is faster than electron-ion).

Under non-equilibrium conditions, the components of the plasma have different temperatures. When time is rescaled to t' and assuming there is no relative drift, the equilibration is described by (Anders 1990)

$$\frac{dT_\alpha}{dt'} = \frac{dt}{dt'}\frac{dT_\alpha}{dt} = \frac{1-v_i/c}{v_i n_{\rm H}(1+f_{\rm He})}\sum_{\beta\neq\alpha}\nu_{\alpha\beta}(T_\beta - T_\alpha), \quad (6)$$

where $\nu_{\alpha\beta}$ is the energy transfer rate between component α and β in physical time. Conservation of energy in the transfer requires the symmetry relation

$$f_\alpha \nu_{\alpha\beta} = f_\beta \nu_{\beta\alpha}. \quad (7)$$

We express the temperature of each IGM component in an array $\mathbf{T}$ and the energy transferring rate in a matrix $\mathbf{M}$. The stiff equilibration can be converted to a matrix operation

$$\begin{aligned}\mathbf{T}(t'+\Delta t') &= \mathbf{T}(t') + \Delta t' \cdot \mathbf{M}\mathbf{T}(t'+\Delta t') \\ &= (\mathbf{I} - \Delta t'\cdot\mathbf{M})^{-1}\mathbf{T}(t'),\end{aligned} \quad (8)$$

where $\mathbf{I}$ is the 5×5 identity matrix, $\mathbf{T}$ has components T_α, $\mathbf{M}$ has entries of some functions of the interaction rate $\tilde{\nu}_{\alpha\beta}$, and $\alpha, \beta \in \{1, 2, ..., 5\}$ denote each IGM species in the order of e^-, H I, H II, He I, and He II. We initialize the temperature of all species with 10^{-6} K, and the final result is insensitive to this initialization. **[Need to make a quantitative statement about this. Also what is the default initial condition for H II and He II fractions.]**

Using Equation (8), it is straightforward to show that $\mathbf{M}$ has the form

$$\mathbf{M} = \begin{pmatrix} -\sum_{\beta\neq1}\nu_{1\beta} & \nu_{12} & \nu_{13} & \nu_{14} & \nu_{15} \\ \nu_{21} & -\sum_{\beta\neq2}\nu_{2\beta} & \nu_{23} & \nu_{24} & \nu_{25} \\ \nu_{31} & \nu_{32} & -\sum_{\beta\neq3}\nu_{3\beta} & \nu_{34} & \nu_{35} \\ \nu_{41} & \nu_{42} & \nu_{43} & -\sum_{\beta\neq4}\nu_{4\beta} & \nu_{45} \\ \nu_{51} & \nu_{52} & \nu_{53} & \nu_{54} & -\sum_{\beta\neq5}\nu_{5\beta} \end{pmatrix}, \quad (9)$$

The row summations vanish because $dT_\alpha/dt' = 0$ whenever all of the components are in equilibrium at the same temperature. **[please check you agree with the reason]**

[* I have gone through here. ***]**

The above-mentioned stiff solver is implemented in the code as follows. Equation 1 to 3 forms a system of $3N_{\rm grid}$ ordinary differential equations describing the thermalization of electrons. This can be solved by first-order Euler method doing integrations on rescaled time step. At each time step, a net amount of energy enters photoelectrons (Equation 3) by photoionization. Electrons then transfer heats into rest IGM species via the matrix transformation in Equation 8.

The natural next step is calculating the entries of $\mathbf{M}$. We discuss the interactions between different IGM components in the following four categories.

3.1. *Ionized + Ionized*

Ionized particles include e^-, H II, and He II. For two-body system, the corresponding energy transfer rate is (Anders 1990)

$$\nu_{\alpha\beta} = \frac{(m_\alpha m_\beta)^{1/2} Z_\alpha^2 Z_\beta^2 n_\beta \ln\Lambda_{\alpha\beta}}{(m_\alpha T_\beta + m_\beta T_\alpha)^{3/2}} \cdot 1.8\times10^{-19}\ \sec^{-1}, \quad (10)$$

where $m_{\alpha/\beta}$ are the particle mass of α and β respectively, $Z_{\alpha/\beta}$ are their atomic numbers, n_β is the particle density of β, and temperature is in eV. $\ln\Lambda_{\alpha\beta}$ is the Coulomb logarithm, where we fix its value to 28 in this calculation with the following reasoning. By definition (Book 1983), $\ln\Lambda_{\alpha\beta} = \ln(b_{\rm max}/b_{\rm min})$, where $b_{\rm max}$ is the maximum impact parameter (equals to debye length) and $b_{\rm min} = e^2/(2\pi\epsilon_0 m_e v_e^2)$ is the minimum impact parameter. Since the coulomb logarithm does not vary much in the temperature range of reionization, we fix its value to 28 by assuming a characteristic temperature 10,000 K.

3.2. *Ions + Neutrals*

For ions (H II and He II) and neutrals (H I and He I), their mutual interactions are primarily caused by the the polarization of neutrals induced by the electric field of ions, and resonant exchange for species with same atomic number. The energy transfer rate $\nu_{\alpha\beta}$ is related to the interaction cross section $\sigma_{\alpha\beta}$ through

$$\nu_{\alpha\beta} = n_\beta \frac{2m_\alpha}{m_\alpha + m_\beta} \nu_{\alpha\beta,p}, \tag{11}$$

where $n_{\rm neutral}$ is the neutral density, $\nu_{\alpha\beta,p} \equiv \langle \sigma_{\alpha\beta} v \rangle$ is the momentum transfer rate, v is relative speed, and the factor of mass ratio is introduced by the conversion from momentum to energy transfer rate. Here we assume energy transfers from α to β. Since $p_\alpha \nu_{\alpha\beta,p} = p_\beta \nu_{\beta\alpha,p}$, and ions possess much momentum for the same velocity, we have $\nu_{\alpha\beta,p} = \nu_{\beta\alpha,p} m_\beta / m_\alpha$. Therefore, energy transfer rate $\nu_{\alpha\beta}$ is identical under the exchange of species.

Assuming the polarization potential is in an ideal r^{-4} form, the momentum transfer rate coefficient is a constant (Draine 2011). For resonant exchange (H I + H II, He I + He II), we fit the total cross section as a function of temperature in a power law form, using data from Hunter & Kuriyan (1977) and Maiorov et al. (2017).

3.3. *Electrons + Neutrals*

For interactions between electrons and neutrals, we also use a power-law fitting for the elastic collisions cross section. Experimental data is measured by Brackmann et al. (1958) and Golden et al. (1984).

3.4. *Neutrals + Neutrals*

Due to the van der Waals interaction caused by dipole moment fluctuations, neutrals repulse each other at small range and weekly attract at larger separation. We do the power-law fitting for the elastic scattering cross section according to the measurements from Gengenbach et al. (1973).

The interpolated interaction rates between IGM pairs as a function of temperature are shown in Figure 1. Electron-ion and ion-ion interactions dominate in low-temperature region (less than 10^4 K) and decrease to become comparable with electron/ion-neutral rate.

4. RESULT

In this report, we aim to quantify the dependence of $T_{\rm re}$ on the incident spectrum temperature $T_{\rm bb}$ and front velocity v_i when non-equilibrium interactions are present. The results are summarized from Figure 2 to 6. In Figure 2, $T_{\rm re}$ gets higher with higher velocity (lower density) because of the greater effect of Lyman-α cooling process.

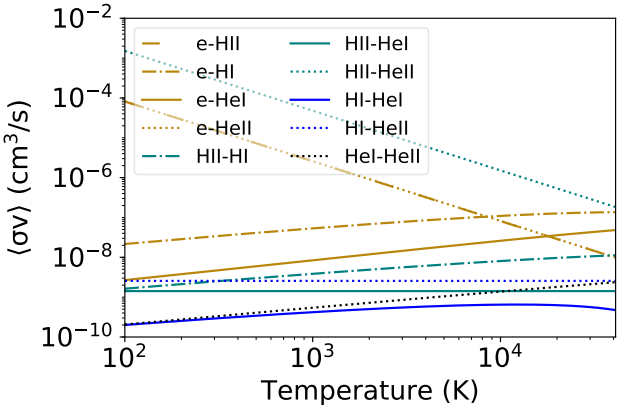

Figure 1. The interaction rates between different IGM species, interpolated from the experimental data listed in sections 3.

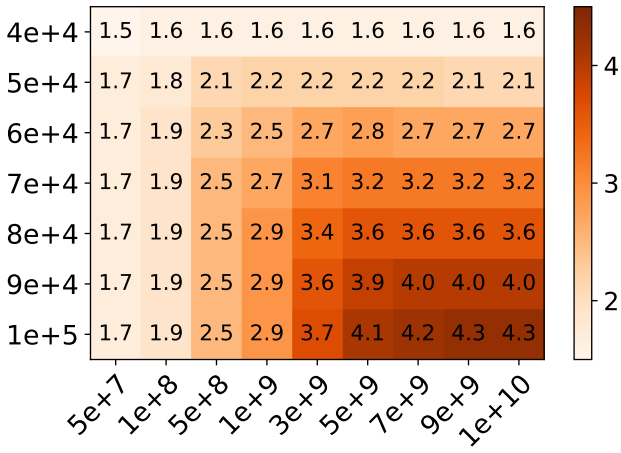

Figure 2. $T_{\rm re}$ in 10^4 K as a function of ionization photon temperature $T_{\rm bb}$ (vertical, in K) and front velocity v_i (horizontal, in cm/s). The mutual interactions between species are included.

Figure 3 illustrates a few examples of the equilibration process by inputing multiple combinations of reionization parameters, where the ionizing sources inject radiation from the left of the plot, and the ionization front propagates towards right. Photoelectrons stream ahead of the ionization front and heats up the rest species by collisions.

In general, all species stay in equilibrium at fully-ionized region (roughly $N_{\rm H} \lessapprox 25 \times 10^{18}$ cm^{-2} in Figure 3). Note that non-equilibrium interactions are proportional to the density, which scales inversely with v_i. Therefore, compared with the equilibrium case (solid green curve in Figure 3), $T_{\rm re}$ gets lowered when non-equilibrium interactions (the rest curves) are present. At hight-velocity ($v_i \gtrapprox 10^8$ cm/s) region, temperatures of electrons and ions decouple from neutral species in the

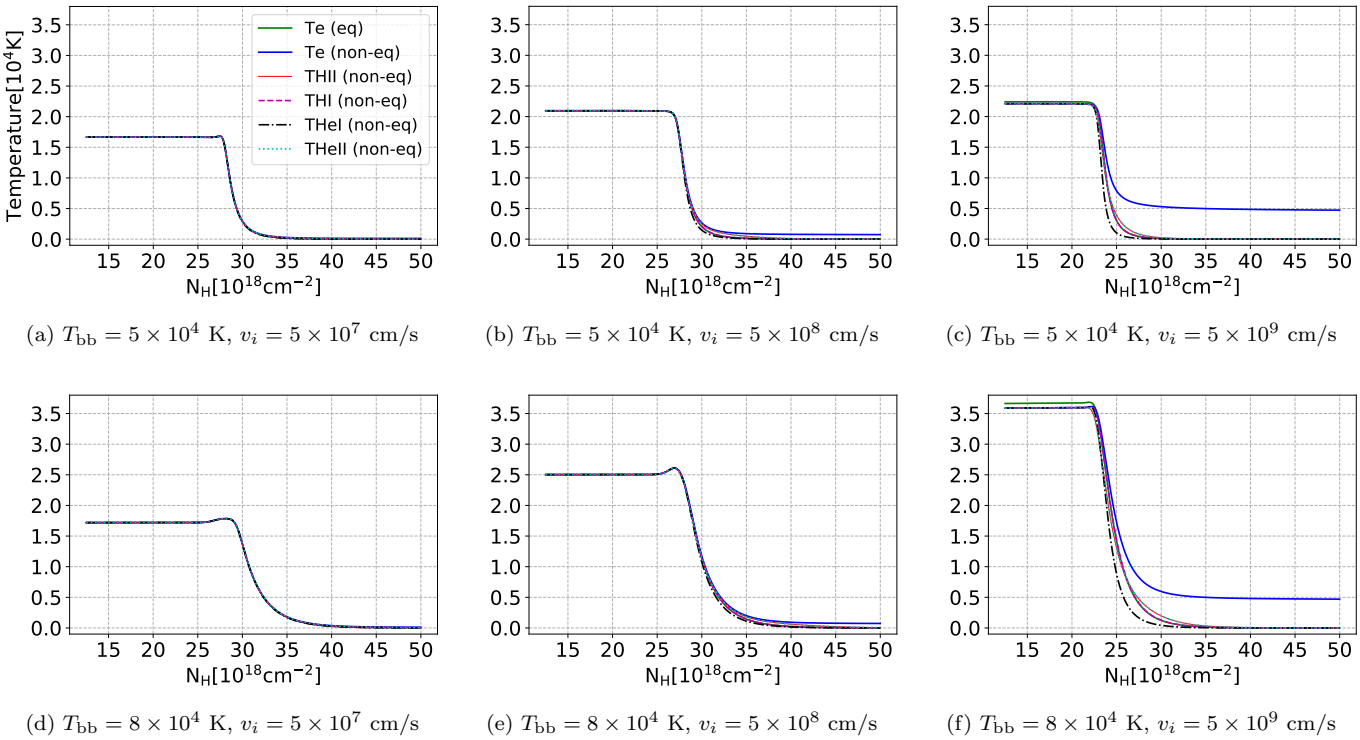

(a) $T_{\rm bb} = 5 \times 10^4$ K, $v_i = 5 \times 10^7$ cm/s (b) $T_{\rm bb} = 5 \times 10^4$ K, $v_i = 5 \times 10^8$ cm/s (c) $T_{\rm bb} = 5 \times 10^4$ K, $v_i = 5 \times 10^9$ cm/s

(d) $T_{\rm bb} = 8 \times 10^4$ K, $v_i = 5 \times 10^7$ cm/s (e) $T_{\rm bb} = 8 \times 10^4$ K, $v_i = 5 \times 10^8$ cm/s (f) $T_{\rm bb} = 8 \times 10^4$ K, $v_i = 5 \times 10^9$ cm/s

Figure 3. Temperature evolution of species at ionization front with different incident blackbody radiation fields $T_{\rm bb}$ and front velocities v_i. $T_{\rm re}$ refers to the plateau at $N_{\rm H} \lessapprox 25 \times 10^{18}$ cm^{-2}. Solid green curves assume IGM is always in equilibrium state, and other curves represent the temperature of each species when mutual interactions are included. In general, the non-equilibrium effects become stronger at higher velocity and temperature because the interaction rate gets smaller according to Equation 6. For these typical incident radiations and front velocities, the final temperatures with interactions get lowered compared with the equilibrium case.

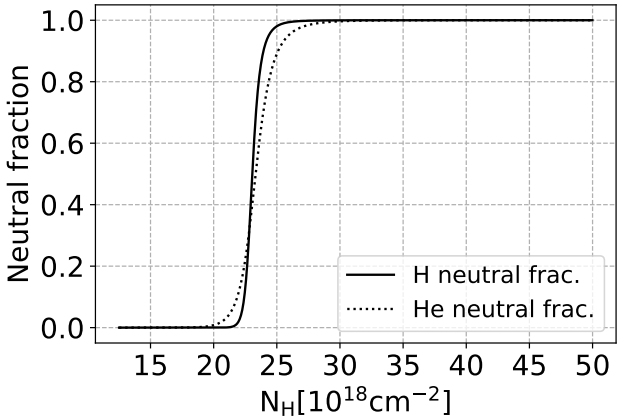

Figure 4. Neutral fraction of hydrogen and helium with $T_{bb} = 5 \times 10^4$K and $v_i = 5 \times 10^9$cm/s K.

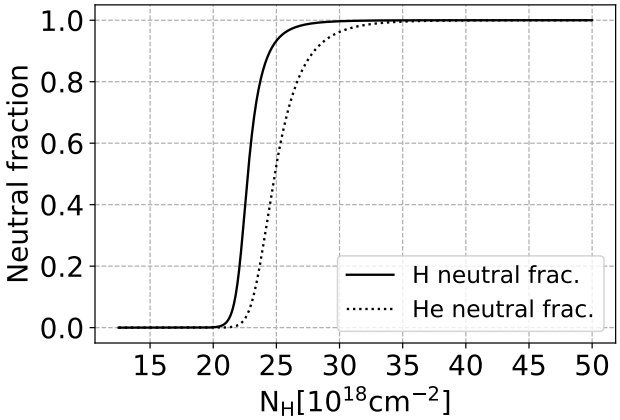

Figure 5. Neutral fraction of hydrogen and helium with $T_{bb} = 8 \times 10^4$K and $v_i = 5 \times 10^9$cm/s K.

ionization front, and non-equilibrium effects becomes important.

Here we make an order-of-magnitude estimation on the non-equilibrium states for IGM species outside the I-front. At $T_{bb} = 5 \times 10^4$ K and $v_i = 5 \times 10^9$ cm/s (Figure 3f), for example, we can take two reference points along the propagation path: $N_{\rm H,1} = 2.0 \times 10^{19}$ cm^{-2} and $N_{\rm H,2} = 3.5 \times 10^{19}$ cm^{-2}. These two correspond to fully ionized and neutral regions in Figure 5. The change of hydrogen column density is therefore $\delta N_{\rm H} =$

1.5×10^{19} cm^{-2} (use lower case delta here to distinguish from the grid size in the previous section). The change of helium column density is of order $\delta N_{\rm He} \approx 10^{18}$ cm^{-2} since there are roughly a few helium atoms per hundred hydrogen atoms. At $N_{\rm H,2}$, electrons are thermalized to 5×10^3 K before I-fronts arrive. This is due to two factors: I-front velocity v_i and average interaction rate $\bar{\nu}$ between electron and other species. In this case, the I-front is propagating fast enough that electrons do not have enough time to reach equilibrium with IGM. Photons between 1 to 4 Ry stream from $N_{\rm H,1}$ to $N_{\rm H,2}$. Due to photoionization, the medium between $N_{\rm H,1}$ and $N_{\rm H,2}$ is optically thick to low-energy photons and relatively thin to those with high energy. We estimate that the average photon energy deposit into an electron is $E_{e,\rm inject} = 2.5$ Ry. As a result, the faster electrons interact with IGM species, the less energy remains in electrons before I-front arrives:

$$E_{e,\rm remain} = E_{e,\rm inject} \cdot \frac{\Delta t_{\rm cool}}{\Delta t_{\rm front}} = E_{e,\rm inject} \cdot \frac{\delta \bar{N}_{\rm cool}}{\delta \bar{N}_{\rm front}} \quad (12)$$

where $\Delta t_{\rm cool} \equiv 1/(n_{\rm H}\bar{\nu})$ is the average time that electrons cool down due to collisional interactions, $\Delta t_{\rm front}$ is the time that I-front propagate from $N_{\rm H,1}$ to $N_{\rm H,2}$, $\delta \bar{N}_{\rm front} \equiv (\delta N_{\rm He} + \delta N_{\rm H})/2 \approx 5 \times 10^{18}$ cm^{-2} is the average change of neutral column density, $\delta \bar{N}_{\rm cool} \equiv v_i \Delta t_{\rm cool} n_{\rm H} = v_i/\bar{\nu}$ is the average change of column density when electron transfer heats to the rest species. At 5×10^3 K, electrons mainly interact with the rest four species with an average energy transfer rate $\bar{\nu} = 5 \times 10^{-8}$ cm^{3}s^{-1}. This can be verified by referring to the yellow curves at 5×10^3 K in Figure 1 (note that there is an conversion factor of $m_e/(m_e + m_i)$ from $\langle \sigma_{\alpha\beta} v \rangle$ to $\nu_{\alpha\beta}$ for $e-$H I and $e-$He I interactions). Therefore $\delta \bar{N}_{\rm cool} = 10^{17}$ cm^{-2}, and $E_{\rm e,remain} = 5 \times 10^{-2}$ Ry. Figure 3 (f) shows that $E_{\rm e,remain} \approx 5 \times 10^{-2}$ Ry (5×10^3 K) which is the same order as we predicted.

In the temperature and velocity range of interests, ions (H II and He II) stay in equilibrium all the time since their mutual interaction rate is high enough compared with the front propagation speed.

Naturally, the final temperature within the reionization bubble increases as the incident blackbody temperature ($T_{\rm bb}$) becomes stronger. However, the result gets more complicated when non-equilibrium interactions are taken into account (Figure 6). This is because ion-neutral interaction and electron-ion interaction scale differently with temperature in the power-law model fitting. Ion/electron-neutral interaction rate scales with $T^{1/2}$ while electron-ion interaction rate scales with $T^{-3/2}$. Therefore, for low-temperature incident radiation ($T_{\rm bb} \lessapprox 5 \times 10^4$ K) electron-ion interaction rate is the larger in I-front, and electron/ion-neutral interaction becomes more significant at higher temperature ($T_{\rm bb} \gtrapprox 7 \times 10^4$ K). At $T_{\rm bb} \approx 6 \times 10^4$ K, both interaction rates are relatively low compared with timescale that particles stay in the I-front, so $T_{\rm re}$ decreases the most compared with the equilibrium case.

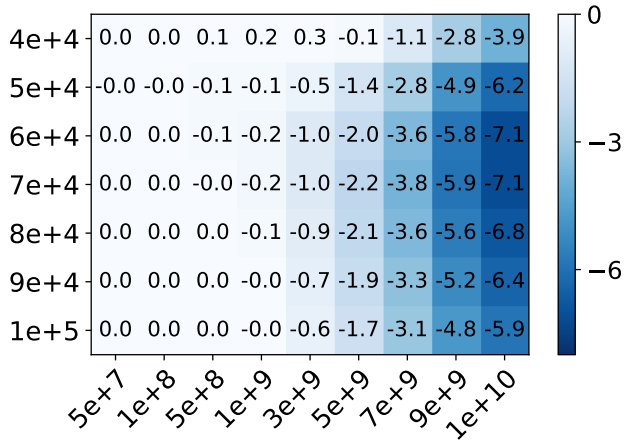

Figure 6. Relative difference (in percentage) between $T_{\rm re}$ with and without non-equilibrium effects. Blue color indicates that interactions decrease $T_{\rm re}$. Vertical axis is the incident photon temperature in K assuming blackbody spectrum, and horizontal axis represents I-front velocity in cm/s....

In our model, the collective effect of incident radiation and front velocity on the ionization front creates a region ($T_{\rm bb} \approx 6 \times 10^4$ K, $v_i \approx 1 \times 10^{10}$ cm/s) in the heat map where the difference of $T_{\rm re}$ between equilibrium and non-equilibrium cases is the largest ($\sim 10\%$, and $T_{\rm re} \approx 2.6 \times 10^4$ K). The bounds of the heat map are limited by our choice of energy sources for reionization. The upper limit of temperature we adopt (10^5 K) corresponds to the effective blackbody temperature of the generic spectra for metal-free stars above $100 M_\odot$ (Bromm et al. 2001), which is very efficient at ionizing hydrogen and helium.

5. SUMMARY AND CONCLUSIONS

We have presented a model of post-I-front temperatures $T_{\rm re}$ when non-equilibrium interactions between IGM species are present. Existing reionization simulations typically assume that photoelectrons thermalize baryon gas within an I-front in a timescale mush shorter than the time over which the baryon species stays inside the front. Namely, the equilibration condition is assumed to be established instantaneously in the I-front (referred to as equilibration assumption). With this assumption, all species can reach the same temperature immediately as I-front passes by.

To verify equilibration assumption and better predict $T_{\rm re}$, this paper made a first attempt to combine density-dependent ionization front model with an implicit stiff solver to include baryons elastic interactions. Our main results are as follows:

1. Equilibration assumption is still valid in the region where I-front moves below 10^9 cm/s. However, baryon species start to thermally decouple at higher-velocity (lower-density) region, where the momentum and energy transfer rates are comparable with the front speed. This can be illustrated by Figure 3 (c) and (f). Photoelectrons first heat up ions and H I through elastic collisions, and He I is the last to be thermalized due to its small momentum transfer cross section.

2. Adding non-equilibrium effects, this density-dependent model still predicts final temperature $T_{\rm re}$ decreases as local density Δ increases (or I-front velocity v_i increases), because of the greater importance of the collisional cooling effects (Figure 2). $T_{\rm re}$ ranges from 1.5×10^4 K to 4.3×10^4 K in our parameter space.

3. We demonstrated that during the EoR, the non-equilibrium interactions will affect $T_{\rm re}$ up to a level of 7%. Higher-velocity (lower-density) region has smaller momentum transfer rate, so baryons species have lower temperatures than photoelectrons in the ionization front. Therefore, photoelectrons will be averaged to a lower final temperature than the equilibrium case. Compared with the equilibrium model, $T_{\rm re}$ is decreased around ten percents at the region $v_i \gtrapprox 10^9$ cm/s (Figure 6), where $T_{\rm re}$ is approximately between 2.2×10^4 K and 4.3×10^4 K. $T_{\rm re}$ is lowered more rapidly as v_i gets closer to the speed of light.

Future improvements include a better interpolation of the momentum transfer cross section and using a realistic incident spectrum (e.g. quasar spectrum) instead of blackbody, and a two-dimensional grid model to better describe inhomogeneous ionized bubble.

6. ACKNOWLEDGEMENT

We thank Anson D'Aloisio, Kevin Ingles, and Paulo Montero-Camacho for very useful discussions. This work is supported by...

REFERENCES

Anders, A. 1990, A Formulary for Plasma Physics

Becker, R. H., Fan, X., White, R. L., et al. 2001, AJ, 122, 2850

Becker, G. D., Bolton, J. S., Haehnelt, M. G., et al. 2011, MNRAS, 410, 1096

Boera, E., Murphy, M. T., Becker, G. D., et al. 2014, MNRAS, 441, 1916

Bolton, J. S., Becker, G. D., Haehnelt, M. G., et al. 2014, MNRAS, 438, 2499

Brackmann, R. T., Fite, W. L., & Neynaber, R. H. 1958, Physical Review, 112, 1157

Bromm, V., Kudritzki, R. P., & Loeb, A. 2001, ApJ, 552, 464

Draine, B. T. 2011, Physics of the Interstellar and Intergalactic Medium (Princeton: Princeton University Press)

D'Aloisio, A., McQuinn, M., Maupin, O., Davies, F. B., Trac, H., Fuller, S., & Upton Sanderbeck, P. R. 2019, ApJ, 874, 154

Fan, X., Strauss, M. A., Becker, R. H., et al. 2006, AJ, 132, 117

Garzilli, A., Bolton, J. S., Kim, T.-S., et al. 2012, MNRAS, 424, 1723

Gengenbach, R., Hahn, C., & Toennies, J. P. 1973, PhRvA, 7, 98

Golden, D. E., Furst, J., & Mahgerefteh, M. 1984, PhRvA, 30, 1247

Hirata, C. M. 2018, MNRAS, 474, 2173

Hu, W., Fang, D., Wang, Y., & Yang, F. 1994, PhRvA, 49, 989

Hui, L., & Gnedin, N. Y. 1997, MNRAS, 292, 27

Hunter, G., & Kuriyan, M. 1977, Proceedings of the Royal Society of London Series A, 353, 575

Lidz, A., Faucher-Giguère, C.-A., Dall'Aglio, A., et al. 2010, ApJ, 718, 199

Maiorov, S. A., Kodanova, S. K., Golyatina, R. I., & Ramazanov, T. S. 2017, Physics of Plasmas, 24, 063502

McGreer, I. D., Mesinger, A., & D'Odorico, V. 2015, MNRAS, 447, 499

McQuinn, M. 2016, ARA&A, 54, 313

Miralda-Escudé, J., & Rees, M. J. 1994, MNRAS, 266, 343

Book, D. L. 1983, Naval Research Lab. Report

Planck Collaboration, Aghanim, N., Akrami, Y., et al. 2018, arXiv e-prints, arXiv:1807.06209

Puchwein, E., Haardt, F., Haehnelt, M. G., et al. 2019, MNRAS, 485, 47

Rudie, G. C., Steidel, C. C., & Pettini, M. 2012, ApJL, 757, L30

Schaye, J., Theuns, T., Rauch, M., et al. 2000, MNRAS, 318, 817

Shin M.-S., Trac H., Cen R., 2008, ApJ, 681, 756

Upton Sanderbeck, P. R., D'Aloisio, A., & McQuinn, M. J. 2016, MNRAS, 460, 1885